Comparing Meso-Micro Methodologies for Annual Wind Resource Assessment and Turbine Siting at Cabauw

Rodrigo, J. Sanz; Arroyo, R. Chávez; Gancarski, P.; Guillén, F. Borbón; Avila, M.; Barcons, J.; Folch, A.; Cavar, D.; Allaerts, D.; Meyers, J.

Total number of authors:
11

Published in:
Journal of Physics: Conference Series

Link to article, DOI:
10.1088/1742-6596/1037/7/072030

Publication date:
2018

Document Version
Publisher's PDF, also known as Version of record

Comparing Meso-Micro Methodologies for Annual Wind Resource Assessment and Turbine Siting at Cabauw

Comparing Meso-Micro Methodologies for Annual Wind Resource Assessment and Turbine Siting at Cabauw

J Sanz Rodrigo[1], **R Chávez Arroyo**[1], **P Gancarski**[1], **F Borbón Guillén**[1]

M Avila[2], **J Barcons**[2], **A Folch**[2]

D Cavar[3]

D Allaerts[4], **J Meyers**[4]

A Dutrieux[5]

[1]National Renewable Energy Centre (CENER), Sarriguren, Spain
[2]Barcelona Supercomputing Centre, Barcelona, Spain
[3]Technical University of Denmark, Roskilde, Denmark
[4]KU Leuven, Leuven, Belgium
[5]ATM-PRO sprl, Nivelles, Belgium

Abstract. A summary of the initial results of the "NEWA Meso-Micro Challenge for Wind Resource Assessment" is presented. The objective of this activity, conducted in the context of the New European Wind Atlas (NEWA) project, is to establish a process for the evaluation of meso-micro methodologies in the context of wind resource and wind turbine site suitability assessment. A hierarchy of methodologies that rely on coupling mesoscale and microscale models is evaluated as a tradeoff between accuracy and computational cost in terms of relevant wind conditions for wind turbine siting such as annual energy production, turbulence intensity, etc. Besides integrated annual quantities, these metrics are analyzed in terms of atmospheric boundary-layer drivers at wind climate (mesoscale tendencies) and site characteristics (atmospheric stability). This is used to characterize errors leading to the identification of knowledge-gaps in the model-chain. This first phase of the meso-micro challenge analyzes Cabauw onshore met mast in horizontally-homogeneous conditions to focus the assessment on mesoscale-to-microscale downscaling methods rather than on site complexity. A second phase of the challenge will add sites in heterogeneous terrain conditions from the NEWA database of experiments.

1. Introduction

In the development of meso-micro methodologies for wind resource assessment there is a tradeoff to be made between modeling fidelity and associated cost to yield the required accuracy for the intended use (Figure 1). *Accuracy* is a qualitative concept that is used here to define the closeness of agreement between the predicted quantity of interest and the true value in the real word. Considering wind resource assessment applications, accuracy should gradually improve from the early-stage prospecting phase to the project financing phase, i.e. from *planning* to *bankable* accuracy. This process will hopefully remove the bias and reduce the uncertainty of the assessment to desired financial limits. This typically implies using off-the-shelf wind atlas products, during early planning phase, and design tools of increasing fidelity as the project matures. The required fidelity will depend on the complexity of the

site as illustrated in Figure 1 and is typically limited by the maximum allocated cost in terms of computing time.

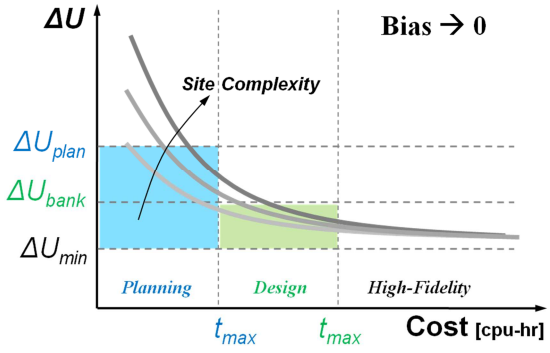

Figure 1. Illustration of the process of improved accuracy ΔU from planning to bankable thresholds (ΔU_{plan} and ΔU_{bank}) against the corresponding maximum allocated computing time cost for different site/flow complexities. Meso-micro methodologies are classified in three large categories depending on the use-case: 1) Wind atlas solutions for spatial planning; 2) RANS-based solutions for wind farm design; and 3) LES-based dynamic downscaling as a high-fidelity reference for engineering tools.

Early-stage spatial planning for wind power deployment is typically done using a wind atlas approach, based on mesoscale model simulations corrected at site level with a linearized model to account for microscale topographic effects on the wind climate. At the other end, high fidelity models are based on the coupling of a mesoscale model with a large-eddy simulation (LES) atmospheric boundary layer (ABL) model that can resolve the dynamic effects of turbulence. Between these two limits, a hierarchy of methodologies is established that combine mesoscale and microscale simulations, ranging in computational cost depending on the type of microscale model (steady or unsteady Reynolds-Averaged Navier Stokes, i.e. RANS or URANS) and the effectiveness of the coupling (dynamical or statistical) [1]. This article provides an assessment of some of these models, being used in the frame of the New European Wind Atlas (NEWA) project, with the objective of defining an open-access evaluation method that can be generally applied in terms of suitable quantities of interest and metrics for wind resource assessment and wind turbine siting applications.

2. The Windbench NEWA Meso-Micro Challenge Phase 1

The objective of the first phase of the *NEWA Meso-Micro Challenge* is to establish an open-access model evaluation process for wind resource assessment methodologies [2]. To this end, a Jupyter notebook based on Python libraries is released with this publication together with the simulation and validation data to allow a traceable assessment process, which will be improved as other sites are added in Phase 2. This initiative is also carried out under the umbrella of the IEA Task 31 Wakebench that aims at establishing a Model Evaluation Protocol and international verification and validation (V&V) strategy for wind farm flow models [3].

Site	Cabauw
Coordinates	51.971ºN, 4.927ºE
Mast height	200 m
Sensors heights	z_S = 10, 20, 40, 80, 140, 200 m z_{WD} = 10, 20, 40, 80, 140, 200 m z_T = 10, 20, 40, 80, 140, 200 m z_{flux} = 3 m
Reference height	z_{ref} = 80 m; z_{flux} = 3 m
Tower shadow sectors	Corrected by using sensors in multiple booms [5]

Table 1. Summary of instrument set-up, where z is the height above ground or sea level, S is the horizontal wind speed, WD is the wind direction, T is the air temperature and z_{ref} and z_{flux} are the reference heights for profile and flux quantities.

The initial focus is based on the well-known Cabauw observatory in the Netherlands. The site is characterized by horizontally-homogeneous conditions with a uniform roughness of z_0 = 0.15 m. Table 1 presents a summary of the instrument set-up at the 200-m mast. Cabauw quality-checked data was obtained from CESAR database [4]. Extensive documentation of the CESAR observatory instrumentation and site characteristics is provided in [5]. Notice that surface turbulence flux

measurements at 3-m height are performed 200 m south of the Cabauw main tower. This avoids significant mast distortion effects at the base of the tower.

All the data has been resampled to hourly time series and reformatted to meet the NetCDF Climate and Forecast (CF) metadata conventions [6].

This work is a follow up of the GABLS3 benchmark, a diurnal cycle at the Cabauw site [7]. The objective of that study was to demonstrate the consistency of different meso-to-micro coupling methods in the transient simulation of a nocturnal low-level jet driven by the interaction between height and time-dependent mesoscale forcing (so called mesoscale tendencies) under a thermally stratified ABL. Microscale ABL models based on URANS (OpenFOAM, Ellipsys and Alya CFD codes) and LES (SP-Wind and Ellipsys) showed similar results than mesoscale simulations with the Weather Research and Forecasting (WRF, [8]) mesoscale model by driving these models with tendencies computed by WRF (as opposed to using idealized inflow conditions). The objective for these models now is to test this meso-micro capability with wind assessment methodologies to produce a year-round characterization of the statistics of siting wind conditions but using a limited number of microscale simulations. The benchmark allows microscale modelers to test their statistical-dynamical methods together with dynamical models that produce time series for the entire year with dynamical downscaling, either using ABL parameterizations based on URANS or explicitly solving turbulence dynamics with LES with horizontal resolutions of less than 1 km.

2.1. Validation Data and Metrics

Relevant quantities of interest for wind resource assessment and site suitability evaluated in this study are:

- Wind speed and wind direction distributions at a reference height of z_{ref} = 80 m as a function of atmospheric stability measured at z_{flux} of 3 m at Cabauw.
- Vertical profiles of wind speed, wind direction, turbulence intensity and potential temperature
- Rotor-based quantities: rotor equivalent wind speed (*REWS*), wind speed shear (α), wind direction veer (ψ) and annual energy production (*AEP*) based on NREL's 5MW reference wind turbine [9] at a hub height of 90 m and with a rotor diameter of 126 m.

The annual energy production (AEP) for a certain bin *k* is calculated by integrating the power curve over the annual wind speed distribution of that sector:

$$AEP_k = T \sum_t P(S_t) f_k(S_t) \tag{1}$$

where T is the length of one year, f_k is the frequency of the bin, $P(S_t)$ and $f(S_t)$ are the power curve and probability density function of the horizontal wind speed S at a timestamp t. The total *AEP* is then calculated by summing up the AEP_k for all the bins, where each bin is defined in terms of intervals of wind speed, wind direction and atmospheric stability.

The capacity factor (*CF*) is the ratio of the AEP to the ideal production resulting from the turbine running at rated power throughout the whole year.

$$CF = \frac{AEP}{T\,P_{rated}} \tag{2}$$

The *REWS* is the wind speed corresponding to the kinetic energy flux through the swept rotor area, when accounting for the vertical shear of wind speed and direction [10]:

$$REWS = \left[\frac{1}{A}\sum_i \left(A_i S_i^3 \cos\beta_i\right)\right]^3 \tag{3}$$

where A is the rotor area and A_i are the horizontal segments that separate vertical measurement points of horizontal wind speed S_i across the rotor plane. The *REWS* is here weighted by the cosine of the angle β_i of the wind direction WD_i with respect to the hub-height wind direction to account for the effect of wind veer [11].

Wind shear exponent α is defined by fitting a power-law curve across the rotor wind speed points S_i:

$$S_i = S_{hub}\left(\frac{z_i}{z_{hub}}\right)^{\alpha} \quad (4)$$

Similarly, wind veer is defined as the slope ψ of the linear fit of the wind direction difference:

$$\beta_i = \psi(z_i - z_{hub}) \quad (5)$$

To evaluate simulations and measurements consistently, these quantities are obtained after resampling, by linear interpolation, velocity and wind direction vertical profiles at 10 points across the rotor area and then computing the *REWS* and the shear functional fits. The suitability of these functions can be determined based on the regression coefficient of the fitting.

The turbulence intensity is obtained from the cup anemometers as the ratio of the standard deviation to the mean horizontal wind speed. Then, standard deviation is computed as a bulk quantity from the turbulent kinetic energy:

$$I = \frac{\sigma_S}{S} \quad (6)$$

Validation results are quantified in terms of the mean BIAS on integrated quantities:

$$BIAS_k = \frac{1}{N_k}\sum_i^{N_k}(\chi_{obs} - \chi_{sim}) \quad (6)$$

where χ is any of the above mentioned quantities of interest, simulated (*sim*) or observed (*obs*), and N_k is the number of samples in the corresponding bin *k*.

These quantities of interest and error metric are evaluated for the annual reference period to obtain global performance indicators which are then categorized in terms of wind direction and stability bins. Atmospheric stability is defined in terms of $\zeta = z/L$, where L is the Obukhov length evaluated at height z based on the friction velocity u_*, kinematic heat flux $\overline{w'\theta'}$ and reference temperature at 2-m level Θ_2.

$$L = \frac{u_*^3}{\kappa\frac{g}{\Theta_2}\overline{w'\theta'}};\ \zeta = \frac{z}{L} \quad (7)$$

Table 2. Stability classes.

unstable (u)	$-20 < \zeta < 0.2$
weakly-unstable (wu)	$-0.2 < \zeta < 0.02$
near-neutral (n)	$0 < \zeta < 0.02$
weakly stable (ws)	$0.02 < \zeta < 0.2$
stable (s)	$0.2 < \zeta < 20$

In this study, bins have been defined based on 30º wind direction width and 5 stability classes (Table 2), following the definition of [12], to make sure each bin in the direction/stability joint distribution has at least 10 samples.

3. Participating Models

Table1 shows a list of the models participating in the model intercomparison benchmark. For simplicity, as it was done in the GABLS3 case, the microscale models assume dry atmosphere throughout the simulation. Then, it is assumed that the effect of humidity, as well as other atmospheric physics that are not simulated explicitly by the microscale models, are indirectly embedded in the mesoscale forcings.

Single-column URANS models are used as proxy to 3D models used in heterogeneous wind conditions. This is a cost-effective solution to test different ABL settings, which can be evaluated against the WRF-YSU reference mesoscale model results to assess consistency with the input forcing and against the SP-Wind LES as a high-fidelity model to evaluate turbulence characteristics. These long-term simulations are brute-force simulations that serve as reference to build statistical

methodologies that can produce relevant long-term statistics by using a reduced number of simulations.

Table 3: Summary of model simulations. Monin-Obukhov similarity theory (MOST) surface boundary conditions use either 2-m (T_2) or skin temperature (T_{SK}) from WRF

Name	Input	Turbulence	*z*-Levels	Surface B.C.
WRF-YSU (ref)	ERA Interim	YSU	46	Noah
CFDWind1D (k-ε)	WRF (ref)	*k-ε*	301	MOST, T_2
Ellipsys1D (k-ε)	WRF (ref)	*k-ε*	192	MOST, T_{SK}
SP-Wind (LES)	WRF (ref)	LES-TKE	200	MOST, T_2

3.1. Reference WRF simulation: Input Data for Microscale Models

For consistency with the GABLS3 precursor benchmark, a similar WRF setup was used in these year-long simulations to produce mesoscale tendencies for the microscale models. WRF-ARW v3.8 [8] was configured with a one-way nesting configuration based on three concentric square domains centred at the sites, as in Kleczek et al [13], based on a 61x61 points grid with 27, 9 and 3 km horizontal resolution. The vertical grid, approximately 13 km high, is based on 46 terrain-following (eta) levels with 24 levels in the first 1000 m, the first level at approximately 13 m, a uniform spacing of 25 m over the first 300 m and then stretched to a uniform resolution of 600 m in the upper part. The U.S. Geological Survey (USGS) land-use surface data, which comes by default with the WRF model, is used together with the unified Noah land-surface model to define the boundary conditions at the surface. Other physical parameterizations used are: the rapid radiative transfer model (RRTM), the Dudhia radiation scheme and the Yonsei University (YSU) first-order PBL scheme [14]. The simulation uses input data from ERA-Interim [15] with a spin-up time of 24 hours initialized every day at 12UTC.

During runtime, mesoscale tendencies are computed and stored in the standard output of WRF. Tendencies from the 3 km domain are averaged horizontally over a square box of 9-km length to filter out small scale fluctuations [16]. A sensitivity study and validation of mesoscale tendencies for the sites of this study is discussed in [17].

3.2. CFDWind

CFDWind1D is a python-based finite-difference code. The single-column model (SCM) is used as a prototype to design the CFDWind 3D model [16]. They are both based on unsteady Reynolds-Averaged Navier Stokes (URANS) equations using the *k-ε* model of Sogachev et al [18] with constants: $C_{\varepsilon 1} = 1.52$, $C_{\varepsilon 2} = 1.833$, $\sigma_k = 2.95$, $\sigma_\varepsilon = 2.95$ and $C_\mu = 0.03$.

The SCM is solved on a 4-km long log-linear vertical grid with 301 levels using a time step of 1 s. Pressure gradient and advection forcings are lumped together as a time and height-dependent equivalent geostrophic wind that enters momentum equations as source terms. The advection temperature tendency is also added as a source term in the potential temperature equation. No-slip conditions are defined for momentum equations at the surface. Surface boundary conditions for potential temperature are defined based on MOST, inferring the surface temperature by prescribing the diurnal 2-m temperature from the mesoscale input data and using the dynamic surface-layer friction velocity and heat flux as described in [16].

3.3. Ellipsys3D

The EllipSys1D [19] code is a one-dimensional version of a more general EllipSys3D CFD code [20][21][21]. The present EllipSys1D based URANS study utilizes *k-ε* model [18], where the same set of constants as the other URANS models in the benchmark was used. The problem is solved on a 6-km high vertical domain with 192 tanh stretched grid points using a time step of 1 s.

A no-slip boundary condition was applied at the surface boundary, with WRF based surface temperature (*TSK*) prescribed as a boundary condition for the potential temperature equation. Momentum advection forcings together with the temperature tendencies are included in the code in a way completely analogous to the procedure presented for the CFDWindSCM code [16].

3.4. SP-Wind

SP-Wind is an in-house pseudo-spectral LES code developed at KU Leuven [22][23][24]. SP-Wind solves the Boussinesq form of the conservation equations for mass, momentum and potential temperature on a three-dimensional Cartesian grid. A fourth-order energy-conservative finite difference scheme is used in the vertical direction, and time integration is performed using a classic four-stage fourth-order Runge—Kutta scheme with a variable time step based on a CFL number of 0.4. The subgrid-scale stress and heat flux are computed with a prognostic TKE model [25], and the surface boundary conditions are imposed using classic Monin-Obukhov similarity theory [26], where corrections for surface-layer stability are included by means of an approximate analytical solution of the implicit flux-profile relationships [27].

A year-long integration is performed for the Cabauw site on a horizontally periodic domain of 4.56x4.56x5 km with 152x152x200 grid points (corresponding to a horizontal grid resolution of 30 m). The vertical grid has a uniform spacing of 15 m in the first 2.25 km, above which it is stretched to a maximum grid size of 75 m (fs=1.06). A Rayleigh damping layer is added above 4 km. The numerical computation is performed on the tier-1 cluster BrENIAC of the Flemish Supercomputer Centre using 12 compute nodes consisting of two 14-core “Broadwell” Xeon E5-2680v4 CPUs, for a total of 336 cores. With this computational set-up, the ratio of wall-clock time to simulated time lies between 0.5 and 1.0. In order to keep the total wall-clock time manageable, the months are simulated in parallel with a spin-up time of 12 hours initialized at 12:00 UTC of the last day of the previous month. Initial profiles, mesoscale tendencies (geostrophic wind and horizontal momentum advection) and surface temperature (inferred from the 2-m temperature) are all extracted from mesoscale WRF simulations as in [16]. Time series of surface-layer parameters and vertical profiles are stored with a sample frequency of 0.1 and 0.017 Hz, respectively.

4. Wind Assessment Methodologies

At this stage, we present results for year-long integrations of the models in Table 2 with the objective of comparing dynamical downscaling methodologies. These brute-force simulations of microscale models will be used as benchmark to build more cost-effective statistical methodologies based on a reduced number of microscale simulations.

For brevity, a reduced set of figures and results are presented in this article, with focus on the Cabauw site and WRF-YSU simulation data, to illustrate the evaluation methodology. The interested reader can explore other results by running the accompanying Jupyter notebook and associated data [28][29].

5. Results

5.1. Annual Distributions

Figure 2 shows histograms of wind speed and direction with bin-based normalized stability distributions according to the classification of Table 2. As expected, as the wind increases neutral stratification tends to be more frequent. Unstable conditions dominate at low wind speeds and stable conditions are more frequent at moderate speeds, between 6 and 11 m s^{-1}. This is particularly important in the SE quadrant where frequent nocturnal low-level jets happen as in the GABLS3 diurnal cycle. The prevailing wind direction sector from SW is characterized by well-mixed conditions, predominantly neutral or unstable. Figure 2 compares the observed distributions with those simulated by the WRF-YSU reference model, each one based on its own assessment of *z/L*. The agreement is reasonably good, especially in regards to the prediction of wind direction and stability classes. This allows us to consider WRF-YSU a valid reference for the evaluation of microscale models.

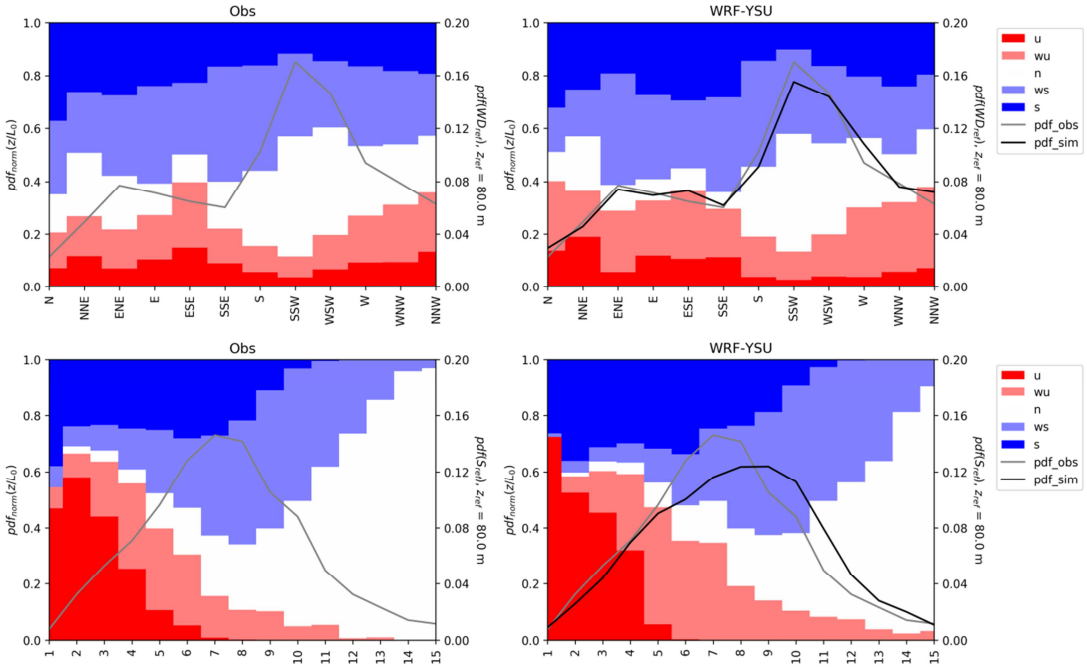

Figure 2. Annual distributions at 80 m of wind direction (top) and wind speed (bottom) with bin-based normalized stability distributions according to the classification of Table 2.

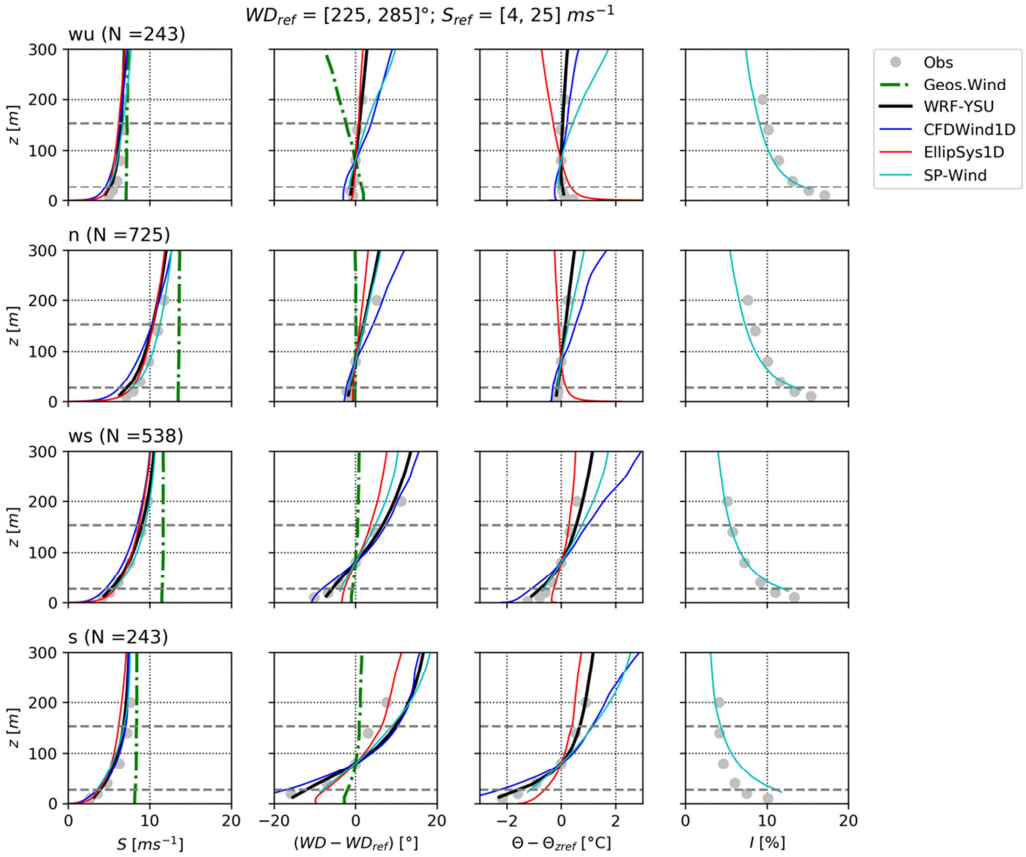

Figure 3. Ensemble-averaged vertical profiles for the prevailing wind direction sector of horizontal wind speed S (left), wind direction difference WD-WD_{ref} and potential temperature difference Θ-Θ_{ref} with respect to a reference height of z_{ref} = 80 m at Cabauw met mast. The geostrophic wind from the reference WRF-YSU simulation is also indicated.

5.2. Vertical Profiles

Figure 3 shows ensemble-averaged vertical profiles of wind speed and wind direction and potential temperature relative to the reference height for the prevailing wind direction sector and different stability classes at the Cabauw site. In this analysis, the time series filtered based on the observed wind speed, direction and stability reference levels. This way we avoid introducing biases due to errors in the simulation of the Obukhov length and we focus the analysis on mean profiles from synchronized samples.

The geostrophic wind speed and direction is also shown to illustrate the changes on the main driving force of the microscale models at different atmospheric conditions. This particular sector is characterized by well-mixed conditions and the geostrophic wind in the first 300 m is relatively uniform in magnitude (low baroclinicity). As expected, when the wind profile switches from unstable to stable conditions the gradient of wind speed and direction increases and turbulence intensity decreases. It is also worth noticing that the potential temperature in neutral conditions is not completely vertical due to the presence of residual nocturnal stable conditions above the surface layer. In stable conditions the 200-m observation level is close to geostrophic conditions.

Microscale models produce very similar velocity profiles following closely the reference WRF results. This is a good indication of long-term equilibrium between the momentum equations at microscale and the input mesoscale tendencies. On the other hand, potential temperature profiles tend to deviate more from the mesoscale reference due to lack of equilibrium in the energy equation, possibly primarily due to the lack of humidity tendencies.

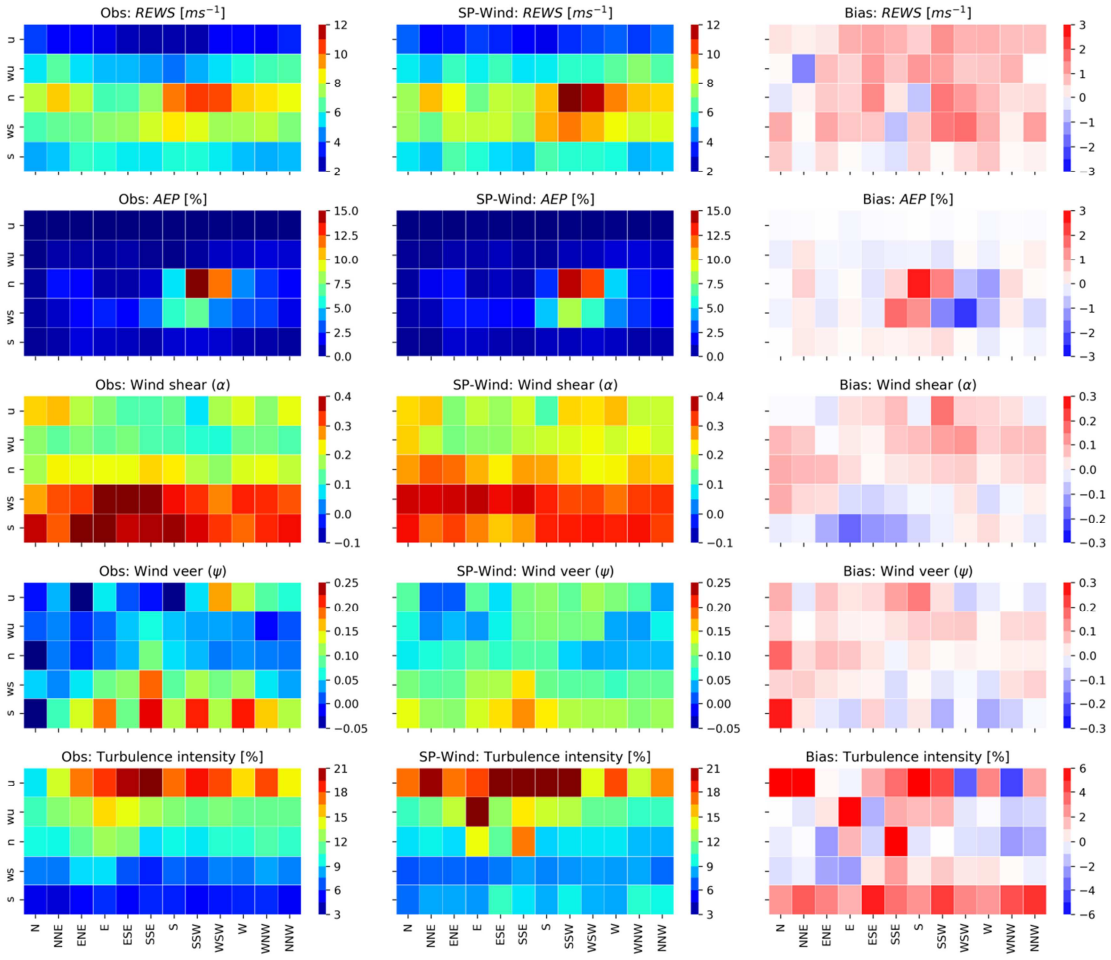

Figure 4. Heatmaps at 80 m level of observed (left), simulated with SP-Wind (middle) and bias (right) of: *REWS*, *AEP*, α wind shear exponent, veer ψ linear-fit slope and turbulence intensity.

5.3. Rotor-Based Quantities of Interest

Figure 4 presents heatmaps of annual bin-averaged quantities of interest and bias between observations and simulations with the SP-Wind model (similar results are obtained with the other models). As in the profile analysis, we use the observed reference levels of stability and wind direction to filter synchronized samples within each bin.

The REWS is larger in neutral and weakly stable conditions peaking on the SSW sector. Since this is also the prevailing wind direction, most of the AEP is concentrated in third windrose quadrant within the neutral and slightly stable classes. The simulation globally underestimates the wind resource consistently with the reference mesoscale simulation that uses as input forcing. The simulation underestimates the largest wind shears in stable conditions but predicts well the directional distribution with a peak on the ESE sector, which is characterized by frequent nocturnal low-level jets. Nevertheless, the underestimation of wind shear in stable conditions does not seem to have a negative impact on the REWS. This is attributed to error compensation in the rotor averaging process.

Turbulence intensity peaks to 21% in the SSE sector under unstable and low wind speed conditions and decreases as low as 4.4% in stable conditions at the NNE sector. SP-Wind tends to overestimate turbulence in both extremes but predicts reasonably well the range of moderate turbulence in near-neutral conditions. The overestimation of turbulence in stable conditions might be due to the relatively coarse resolution of the model (15 m in the vertical) which cannot resolve the fine scales of turbulence that would increase the dissipation rate.

5.4. Annually Integrated Metrics

Annually integrated quantities are computed to quantify the overall performance of the models. These global performance indicators shall be used together with their corresponding heatmaps (Figure 4) to identify potential sources of errors. Sound conclusions about the performance of the models cannot be reached with just one site in simple topographic conditions. This will be the objective of the second phase when sites in different terrain complexities and wind climates will be evaluated. At this stage, this first case of the "NEWA Meso-Micro Challenge" has been used to establish an evaluation methodology for meso-micro methodologies.

Table 4. Annual bias in % normalized with respect to the observed quantity of interest.

	REWS	S_{hub}	***CF***	α **(shear)**	ψ **(veer)**
WRF-YSU (ref)	7,48	7,30	18,16	-3,85	21,91
CFDWind1D (k-ε)	10,22	9,58	21,61	12,63	74,75
Ellipsys1D (k-ε)	3,59	3,12	7,85	-16,65	-10,84
SP-Wind (LES)	9,78	9,52	20,42	6,07	15,85

In this particular case we can observe that the reference WRF simulation was not particularly good in the assessment of the annual wind resource with more than 7% overestimation in the annual *REWS*. This bias is propagated to the microscale models through the input mesoscale tendencies. Nevertheless, these initial results are promising showing a reasonably good consistency with the parent mesoscale simulation.

6. Conclusions and Outlook

The first phase of the NEWA Meso-Micro Challenge for wind resource assessment methodologies has been launched to establish a validation process that enables model developers to design downscaling methodologies. Initial results are presented for dynamical downscaling methods that simulate time series for the whole evaluation period. These simulations will be used as brute-force references to build more cost-effective physical-statistical methodologies that only use a reduce number of microscale simulations.

Preliminary results are presented for the Cabauw site for two codes implementing the same *k-ε* model, compared with a high-fidelity LES microscale model and the parent WRF mesoscale simulation from

which the input forcing is derived. The microscale models present consistent results at reproducing the annual wind climate distribution and mean velocity profiles. Mean turbulence profiles are also well predicted by SP-Wind LES model which can serve as a reference to build better a k-ε model.

The evaluation method described in this paper will be extended to include other sites in heterogeneous terrain conditions from the NEWA database of experiments [30]. The overall model evaluation process along with the data are published as open-access repositories to contribute to the IEA Task 31 "Wakebench" international V&V framework [28][29].

Acknowledgements
This work is carried out with the support from NEWA (FP7-ENERGY.2013.10.1.2, European Commission's grant agreement number 618122) and MesoWake (FP7-PEOPLE-2013-IOF, European Commission's grant agreement number 624562) EU projects under the umbrella of the International Energy Agency IEA-Wind Task 31 "Wakebench". We would like to acknowledge the Royal Netherlands Meteorological Institute (KNMI) for maintaining the CESAR database. The computational resources and services used by DA and JM were provided by the VSC (Flemish Supercomputer Center), funded by the Research Foundation Flanders (FWO) and the Flemish Government – department EWI.

7. References

[1] Sanz Rodrigo J, Chávez Arroyo R-A, Moriarty P, Churchfield M, Kosović B, Réthoré P-E, Hansen KS, Hahmann A, Mirocha JD, Rife D 2016 Mesoscale to microscale wind farm flow modelling and evaluation. WIREs Energy Environ 6(2):e214, doi:10.1002/wene.214
[2] Sanz Rodrigo 2018 NEWA Meso Micro Challenge. *Windbench*, http://windbench.net/newa-meso-micro-challenge-wind-resource-assessment, last accessed February 2018
[3] Sanz Rodrigo J, Moriarty P. 2015 WAKEBENCH Model Evaluation Protocol for Wind Farm Flow Models. Edition 1. IEA Task 31 Report to the IEA-Wind Executive Committee. May 2015
[4] CESAR 2018 Cabauw experimental site for atmospheric research. http://www.cesar-database.nl, last accessed February 2018
[5] Bosveld F 2018 Cabauw In-situ Observational Program 2000 – Now: Instruments, Calibrations and Set-up. http://projects.knmi.nl/cabauw/insitu/index2.htm, last accessed February 2018
[6] Eaton B, Gregory J, Drach B, Taylor K, Hankin S, Blower J, Caron J, Signell R, Bentley P, Rappa G, Höck H, Pamment A, Juckes M, Raspaud M 2018 NetCDF Climate and Forecast (CF) Metadata Conventions Version 1.7. http://cfconventions.org, last accessed February 2018
[7] Sanz Rodrigo J, Allaerts D, Avila M, Barcons J, Cavar D, Chávez Arroyo R, Churchfield M, Kosović B, Lundquist JK, Meyers J et al. 2017 Results of the GABLS3 diurnal cycle benchmark for wind energy applications. *J. Phys.: Conf. Ser.* **854** 012037, doi :10.1088/1742-6596/854/1/012037
[8] Skamarock WC, Klemp JB, Dudhia J, Gill DO, Barker DM, Duda MG, Huang X-Y, Wang W and Powers JG 2008 A description of the advanced research WRF version 3, Technical Note NCAR/TN-475+STR, NCAR, Boulder, CO, June 2008.
[9] Jonkman J, Butterfield S, Musial W and Scott G 2009 Definition of a 5-MW Reference Wind Turbine for Offshore System Development. Technical Report NREL/TP-500-38060, February 2009, https://www.nrel.gov/docs/fy09osti/38060.pdf, last accessed February 2018
[10] Wagner R, Cañadillas B, Clifton A, Feeney S, Nygaard N, Martin CSt, Tüxen E and Wagenaar JW 2014 Rotor equivalent wind speed for power curve measurement – comparative exercise for IEA Wind Annex 32. J. Phys. Conf. Ser. 524: 012108, doi: 10.1088/1742-6596/524/1/012108
[11] Choukulkar A, Pichugina Y, Clack CTM, Calhoun R, Banta R, Brewer A and Hardesty M 2015 A new formulation for rotor equivalent wind speed for wind resource assessment and wind power forecasting. Wind Energy 19: 1439–1452, doi:10.1002/we.1929
[12] Sanz Rodrigo J, Cantero E, García B, Borbón F, Irigoyen U, Lozano S, Fernandes P-M, Chávez RA (2015) Atmospheric stability assessment for the characterization of offshore wind conditions. Journal of Physics: Conference Series 625: 012044, doi:10.1088/1742-6596/625/1/012044

[13] Kleczek MA, Steeveneveld GL and Holtslag AAM 2014 Evaluation of the Weather Research and Forecasting Mesoscale Model for GABLS3: Impact on Boundary-Layer Schemes, Boundary Conditions and Spin-Up. Boundary-Layer Meteorol. 152: 213-243, doi: 10.1007/s10546-014-9925-3
[14] Hong S-Y and Noh Y 2006 A New Vertical Diffusion Package with an Explicit Treatment of Entrainment Processes. Mon. Wea. Rev., 134: 2318–2341, doi: 10.1175/MWR3199.1
[15] Dee DP et al. 2011 The ERA-Interim reanalysis: Configuration and performance of the data assimilation system. Quart. J. R. Meteorol. Soc. 137: 553-597, doi: 10.1002/qj.828
[16] Sanz Rodrigo J, Churchfield M and Kosović B 2017 A methodology for the design and testing of atmospheric boundary layer models for wind energy applications. *Wind Energ. Sci*. **2**: 1-20, doi:10.5194/wes-2-1-2017
[17] Chávez Arroyo RA, Irigoyen Indave A, Sanz Rodrigo J 2018 Analysis and validation of Weather Research and Forecasting model tendencies for meso-to-microscale modelling of the atmospheric boundary layer. J. Phys. Conf. Ser., current issue
[18] Sogachev A, Kelly M and Leclerc MY 2012 Consistent Two-Equation Closure Modelling for Atmospheric Research: Buoyancy and Vegetation Implementations. *Boundary-Layer Meteorol.* **145**: 307–327, doi:10.1007/s10546-012-9726-5
[19] van der Laan MP and Sørensen NN 2017 A 1D version of EllipSys. Technical Report, DTU Wind Energy E-0141, March 2017
[20] Michelsen JA 1994 Block structured Multigrid solution of 2D and 3D elliptic PDE's. Technical Report AFM 94-06, Technical University of Denmark, Department of Fluid Mechanics, May 1994.
[21] Sørensen NN 1995 General Purpose Flow Solver Applied to Flow over Hills. Risø-R-827-(EN), Risø National Laboratory, Roskilde, Denmark, June 1995
[22] Meyers J, Meneveau C 2010 Large eddy simulations of large wind-turbine arrays in the atmospheric boundary layer. AIAA Paper No. 2010-827, doi:10.2514/6.2010-827
[23] Munters W, Meneveau C and Meyers J 2016 Turbulent inflow precursor method with time-varying direction for large-eddy simulations and applications to wind farms. *Boundary-Layer Meteorol*. **159**: 305-328, doi:10.1007/s10546-016-0127-z
[24] Allaerts D and Meyers J 2017 Boundary-layer development and gravity waves in conventionally neutral wind farms. *J. Fluid Mech.* **814**: 95-130, doi:10.1017/jfm.2017.11
[25] Deardorff J W 1980 Stratocumulus-capped mixed layers derived from a three dimensional model. *Boundary-Layer Meteorol*. **18**: 495-527, doi:10.1007/BF00119502
[26] Moeng C-H 1984 A large-eddy-simulation model for the study of planetary boundary-layer turbulence. *J. Atmos. Sci*. **41**: 2052-2062, doi:10.1175/1520-0469(1984)041<2052:ALESMF>2.0.CO;2
[27] Blümel K 2000 An approximate analytical solution of flux-profile relationships for the atmospheric surface layer with different momentum and heat roughness lengths. *Boundary-Layer Meteorol.* **97**: 251-271, doi:10.1023/A:100270831
[28] Sanz Rodrigo J, Chávez Arroyo RA 2018 NEWA Meso-Micro Challenge Phase 1: Benchmark Evaluation Script v1.0. Zenodo, doi:10.5281/zenodo.1240468
[29] Sanz Rodrigo J, Chávez Arroyo RA, Gancarsky P, Borbón Guillén F, Ávila M, Garcons J, Folch A, Cavar D, Allaerts D, Meyers J, Dutrieux A, Montornès A 2018 NEWA Meso-Micro Challenge Phase 1: Benchmark Data v1.0. B2share, doi: [to be published]
[30] Mann J, Angelou N, Arnqvist J, Callies D, Cantero E, Chávez Arroyo R, Courtney M, Cuxart J, Dellwik E, Gottschall J et al. 2017 Complex terrain experiments in the New European Wind Atlas. *Phil. Trans. R. Soc. A.* 20160101, doi: 10.1098/rsta.2016.0101